CFD Model for the Design of Large Scale Flotation Tanks for Water and Wastewater Treatment

M. Kostoglou, T. D. Karapantsios,* and K. A. Matis

Division of Chemical Technology, Department of Chemistry, University Box 116, Aristotle University of Thessaloniki, 541 24 Thessaloniki, Greece

A CFD model incorporating flotation kinetic expressions is developed to simulate the performance of flotation tanks utilized in water and wastewater treatment plants. The focus here is on tanks that operate without any external means of flow mixing (impeller, etc.), such as Dissolved Air Flotation (DAF) tanks, where bubble buoyancy, particle settling, and turbulence are mechanisms contributing comparably to local flotation rates. These flotation mechanisms are analyzed, and the variation of their relative contribution with respect to basic parameters of the flotation process is examined. To increase the computation efficiency, realistic assumptions are made regarding the fluid dynamics and particle conservation issues of the model, and CFD simulations are performed in a two-dimensional frame of reference. Simulation results demonstrate the existence of a complex interaction between tank hydrodynamics and local flotation rates which lead to particle removal efficiencies that could never be invoked by flotation theories alone.

Introduction

Flotation technology is frequently applied in water and wastewater treatment. Solid particulate contaminated water enters the flotation tank where small diameter air bubbles are injected and mixed with it. Flow mixing enhances bubble dispersion and keeps the solid particles in suspension although the suspension may not be uniform, with the larger heavier particles tending to remain in the lower parts of the tank. Rising bubbles collide with suspended particles and adhere to those that have the appropriate surface characteristics. Each bubble can have many encounters with particles and can carry many of them during its rise. As long as there is a net buoyancy force acting on the bubble/particles aggregates, they can separate from the main flow and gather at the free surface of the tank from where they can be subsequently removed. As long as the concentration of bubbles, particles, and bubble/particles aggregates in the flotation tank is low, water flow is dominant and determines the general flow pattern in the tank. Nevertheless, the movement of bubbles, particles, and aggregates creates drag on the water flow and vice versa, the extent of which influences flotation performance.[1,2]

A flotation tank can be thought of as consisting of two basic regions: a "noisy" reaction zone and a "quiet" flotation zone. In the reaction zone, released bubbles are brought vividly in contact with the incoming contaminated water. Particles and bubbles attach in this region. In the flotation zone, the bubble/particles aggregates are allowed to rise, thus separating the solids from the main water stream.

Following the evolution of CFD codes in the past decade, several investigators have employed numerical simulations to examine various aspects of flotation processes. Due to the exceeding computational burden, most of them refer to two-phase (gas−liquid) systems, and only a few attempts have been made with three coexisting phases (gas−liquid−solid). Fawcett[3] studied the two-phase hydraulics (average bubble size 70 μm) of a DAF (Dissolved Air Flotation) tank in a 2D frame of reference using the CFX 4 code. Among the examined parameters (tank dimensions, internal baffle arrangements, water flow rate, and air flow rate) he found that the injected air-to-water flow momentum ratio was the most critical design parameter dictating the effective mixing of air with the main liquid stream.

Hague et al.[4] compared simulations using a k-ϵ turbulence model against laminar flow simulations and, furthermore, against laser Doppler velocimetry data for single- and two-phase flow in a lab scale DAF tank (average bubble size 50 μm) using FLUENT 4.5 code. Strangely, at the quiescent flotation zone of the tank, the turbulent model gave closer agreement with the measured horizontal velocities than the laminar model. This peculiarity should be attributed to the small size of the employed lab scale tank, which did not allow vortices from the reaction zone to sufficiently decay before entering the flotation zone. In another study, Ta et al.[5] simulated a large scale DAF tank (average bubble size 50 μm) incorporating three phases and a 3D structure grid. Air/water flow was described by a Eulerian−Eulerian model, whereas particles were tracked using a disperse Lagrangian model. However, no bubble/particle collision was considered. CFD results were compared with visual information from an underwater camera and an acoustic Doppler velocimetry technique. Overall there was only a qualitative agreement between measurements and predictions with CFD being unable to predict unsteady flow features such as lateral dispersion of bubble clouds.

Working with a dispersed air flotation tank of special design, the so-called Bubble Accelerated Flotation (BAF) tank, Desam et al.[6] undertook a detailed CFD study where the model was validated against measurements from a dye tracing and a photographic technique. The Fluent 5.0 code was used to simulate the flotation zone in 3 dimensions. The effect of bubble diameter as well as the inlet/outlet position and inlet velocity of the air/water mixture in the separation tank were examined and found to be significant on the separation efficiency. Bubbles 250, 500, and 1000 μm were used (one size at a time) in the calculations. A message from their work is that by proper selection of the system geometrical details and further adjustment of the bubble/liquid flow rates it is possible to achieve appreciable mixing of phases and bubble recovery at the tank surface even under reduced shear conditions. This is particularly the case of a DAF tank where the only shearing action is

* To whom correspondence should be addressed. Tel: 0030 2310 99 7772. Fax: 0030 2310 997759. E-mail: karapant@chem.auth.gr.

10.1021/ie0703989 CCC: $37.00
Published on Web 08/24/2007

imposed by the liquid flow as it moves through the reaction zone and mixes with the injected bubbles.

The first time that flotation kinetic concepts such as collision, attachment, and detachment efficiencies were employed in CFD studies was by Koh and co-workers.[7−9] Simulations were performed in 3 dimensions on a Denver-type dispersed air flotation tank using the CFX code and incorporating a turbulent collision model to estimate *locally* the rate of bubble-particle encounters from local values of the turbulent velocity and the size and concentrations of bubbles and particles. It must be stressed though that in Denver-type dispersed air flotation tanks the effect of turbulence is dominant, due to the intense mixing imposed by an impeller, so gravitational/buoyant effects can be safely ignored.

Recent systematic theoretical analyses clearly depicted the various hydrodynamic and physicochemical parameters that dictate flotation performance.[1,2] The extensive interrelationships between parameters acting on different length scales make such models exceedingly complicated to evaluate, and new multiscale generalization concepts have been recently developed in our lab to cope with this issue.[10] Among these parameters, the large scale hydrodynamic features inside a flotation tank have a profound effect on the overall performance of the process.

In water and wastewater treatment often the aim is to remove very small particles (of the order of microns) at low concentrations. For these applications DAF tanks are usually preferred over dispersed air flotation tanks. DAF tanks nominally operate at low hydraulic loads and with bubbles in the range 50−100 μm. Although at such conditions one may assume that the buoyant motion of the bubbles governs the flotation process, it is in fact a serious matter of concern to what extent other mechanisms such as the gravitational motion of particles and turbulence also contribute.

For the past few years we have been investigating the performance of an industrial-scale DAF tank which due to a sudden malfunction of the air injection system is temporarily supplied with large bubbles (100−1000 μm).[11−14] Such ill-functioning may occur when the incoming fluid is highly contaminated with dirt which may partially block the air injection nozzles or/and raise the viscosity of the continuous phase. To our knowledge, this was the first time that flotation kinetic concepts were used in CFD simulations of DAF tanks. It was shown that even under such off-nominal conditions it is still possible to attain reasonable performance by properly adjusting a few operational parameters. The location for air injection, the inclination of an internal baffle of the tank, and the liquid mass flow rate were proposed as such. However, these adjustments complicated further the hydrodynamics in the tank.

The scope of the present work is to develop a relatively simple and robust CFD model capable of predicting the efficiency of particle removal in flotation equipment where different local flotation kinetic mechanisms may play a role. This is the case of, e.g., DAF and BAF tanks where there is no external means of agitating and mixing the three phases (gas/liquid/solid). For this purpose, some intrinsic features of these tanks such as the low particle loading, low turbulence levels, and small particle size are incorporated in the development of the code. A consistent, yet simple, expression (appropriate for incorporation in a CFD code) including different local flotation kinetics does not exist in the literature. It must be stressed though that the present CFD predictions must be seen with reservation until they are validated against experimental results. However, doing measurements in an industrial flotation tank is not a simple issue and requires serious interrupts of the daily operation to implement and validate measurements against standard conditions. Work in that direction is underway.

The structure of the present work is the following: At first, the development of the algorithm is described in detail. More specifically, expressions are derived for the local flotation frequency, the fluid flow model is chosen, and the selection of the appropriate particle conservation equation is explained. Then typical local flotation frequencies attributed to different mechanisms are presented. Finally, a continuous flotation operation is simulated using a commercial CFD code (Fluent) along with a user-defined flotation kinetic subroutine, and the results are presented and discussed. Using this new tool, the performance of the previously studied DAF tank[11−14] was examined as a case study in order to allow comparisons with those earlier results.

Formulation of the Model

Local Flotation Frequency. There are several mechanisms which may eventually lead to the attachment of a solid particle to a bubble. Each of these mechanisms creates a relative motion between the particle and the bubble resulting in an encounter between the two entities. The two major mechanisms responsible for the relative motion between a particle and a bubble are gravity/buoyancy and turbulence. Usually under practical conditions only one of these two mechanisms is important since it dominates over the other. Furthermore, the two mechanisms can be separated in submechanisms which act simultaneously or independently for the generation of bubble-particle aggregates. For example, the gravity/buoyancy mechanism can be divided into the contribution of the buoyant motion of the bubble and the contribution of the gravitational motion (settling) of the particle (simultaneous action). On the other hand, the turbulent mechanism can be divided into the contribution of the motion created by the local fluid velocity (small solid particles, low levels of turbulence) and the contribution of the inertial motion over and above the local fluid velocity (large particles, high levels of turbulence). In the latter case, the two submechanisms do not act simultaneously, but the one prevails over the other depending on the specific turbulent flow field characteristics.

Knowing the particle-bubble encounter rate is not enough to analyze the flotation process. It is important to know what fraction P_c of the encounters leads to collisions and what fraction P_a of these collisions leads to permanent particle-bubble attachment and thus flotation. The quantity P_c is of hydrodynamic nature and at least in principle can be estimated by employing principles of fluid mechanics.[2] On the other hand, the quantity P_a is of physicochemical nature, and so far it can be only estimated from empirical relations or by fitting experimental data. To complete the picture it must be mentioned that the two quantities, P_a and P_c, in general depend on the encounter mechanism.

Keeping in mind the general view of the subprocesses responsible for the flotation process, an expression can be developed for the local flotation frequency appropriately suited to the continuous DAF process examined here. Unlike the case of flotation columns where buoyancy dominates (large bubble size, small turbulence levels) or the case of dispersed flotation cells with intense stirring where turbulence dominates (high turbulence levels), in the case of DAF tanks not only the turbulence level is low since there is no external energy input but also buoyancy is not so large due to the small size of the bubbles. This means that the two mechanisms are of comparable size, and both must be taken into account.

The usual approach is to consider simultaneously the two subterms of the gravity/buoyancy mechanism (bubble and

particle motion) and to derive a combined expression for the collision efficiency P_c. Here the equivalent—but simpler—procedure of examining the two subprocesses independently, each one with its own collision efficiency, is used. With regards to the turbulent flotation submechanisms, only the one corresponding to the low levels of turbulence will be considered here since this is the situation in DAF tanks. In the following, an expression for the collision frequency for each submechanism (buoyant bubble motion, gravitational particle motion, turbulence) will be derived. It is noted that in actual DAF applications, a surfactant (collector) is added to ensure the hydrophobicity of particles so that they can attach stably to bubbles. Thus, in order to focus on the fluid mechanics aspects of the DAF process it is assumed here that $P_a \cong 1$, as it should be for any effective DAF design. Yet, this assumption does not exclude the possibility to vary P_a at subsequent stages of this work.

(i) Collisions Due to Buoyant Motion of a Bubble. The collision frequency is given as

$$K_B = P_{cB}\pi U_b(R_p + R_b)^2 \tag{1}$$

based on simple geometric arguments for the encounter frequency. The encounter frequency is always the product of a geometric effective encounter area and a relative bubble-particle velocity. In eq 1 R_p and R_b are the particle and bubble radii, respectively, U_b is the bubble rise velocity, and P_{cB} is the collision efficiency for the particular mechanism.

The bubble Reynolds number is not very small so Stokes law cannot be used for the computation of U_b. Instead, a procedure proposed by King[1] is employed taking into account that the bubbles used in DAF are not large enough to deviate significantly from the spherical shape. The equations for the computation of U_b for spherical bubbles rising in a stagnant liquid are the following

$$U_b = \left(\frac{8gR_b}{3C}\right)^{1/2} \tag{2}$$

where

$$C = 0.28\left(\frac{(1 + 0.0921f^{1/2})^{1/2} + 1}{(1 + 0.0921f^{1/2})^{1/2} - 1}\right)^2$$

and

$$f = \frac{4}{3}8gR_b^3\left(\frac{\rho}{\mu}\right)^2$$

The density and viscosity of water are denoted as ρ and μ, respectively, and g is the gravitational acceleration.

The particles approach the bubble following the fluid streamlines (except large particles exhibiting inertia; irrelevant to the present application). The fluid streamlines passes by the bubble so the only reason for bubble-particle collision is the finite particle size (interception mechanism). The computation of the collision efficiency, P_{cB}, requires knowledge of the flow field around the bubble. Unfortunately, this flow field cannot be found in closed form since the Reynolds number for the bubble is finite. Yoon and Luttrell[15] developed a composite relation for the flow field based on analytical asymptotic flow fields and interpolation to experimental flow fields. Using the composite flow field, they found for the collision efficiency

$$P_{cB} = \left(\frac{3}{2} + \frac{4}{15}Re^{0.72}\right)\left(\frac{R_p}{R_b}\right)^2 \tag{3}$$

where the Reynolds number for the bubble is defined as $Re = 2U_bR_b\rho/\mu$.

The flow field of Yoon and Luttrell[15] refers to an isolated bubble. Under realistic conditions, however, the local gas volume fraction in the flotation cell can be large enough to allow interaction between the flow fields around each bubble. As a matter of fact, the presence of neighboring bubbles compresses the streamlines toward the bubble leading to increased collision efficiency. A model for the collision efficiency for the case of a nonzero gas volume fraction has been developed by Nguyen[16] based on a bubble-in-cell approach. Here, the equation of Yoon and Luttrell[15] will be corrected in order to account for a finite gas volume fraction by a simple approximation based on the final results of the more complicated model of Nguyen, given in Figure 11.2 ((a) for immobile bubble surface) of ref 2

$$P_{cB} = \left(\frac{3}{2} + \frac{4}{15}Re^{0.72} + 37.5\varphi\right)\left(\frac{R_p}{R_b}\right)^2 \tag{4}$$

where φ is the local gas volume fraction.

(ii) Collisions Due to Gravitational Motion of a Particle. Using the same approach adopted in (i) the collision frequency is given as

$$K_G = P_{cG}\pi u_p(R_p + R_b)^2 \tag{5}$$

In this case, Stokes law can be used for computing the settling velocity u_p of particles since the particle size considered in DAF are small enough to permit this. So for a stagnant liquid

$$u_p = \frac{2}{9}\frac{g(\rho_p - \rho)R_p^2}{\mu} \tag{6}$$

where ρ_p is the density of the particle. The particle trajectories according to this mechanism are always straight lines and are not influenced by the flow field, so $P_{cG} = 1$.

(iii) Collisions Due to Turbulence. According to the phenomenological statistical theories for the homogeneous turbulence,[17] the average relative velocity W between bubble and particle created by the fluid flow fluctuations is

$$W = \frac{5}{\pi}\left(\frac{\epsilon}{15\nu}\right)^{1/2}(R_p + R_b) \tag{7}$$

where ϵ is the turbulent energy dissipation rate, and ν is the kinematic viscosity of the water. Using this velocity the well-known Saffman−Turner[18] relation for the collision frequency (multiplied by a collision efficiency) can be derived:

$$K_T = P_{cT}1.29(R_p + R_b)^3\left(\frac{\epsilon}{\nu}\right)^{1/2} \tag{8}$$

The Saffman−Turner relation has been derived without accounting for the presence of a bubble, and since the existence of a bubble modifies the flow field, a collision efficiency term, P_{cT}, must be incorporated. Yet, the expression for the collision efficiency which is appropriate for the turbulent collision mechanism is a matter of concern. A characteristic comment can be found in a relevant work:[19] "the literature is silent both experimentally and theoretically on these issues at present". In some cases in literature the buoyancy velocity has been used in the turbulent collision efficiency term,[20] but it is obvious that the turbulent velocity from eq 7 is the relevant one. Although some authors have claimed that the flow field for this problem is of an extensional type rather than a uniform one,[21] using the collision efficiency derived

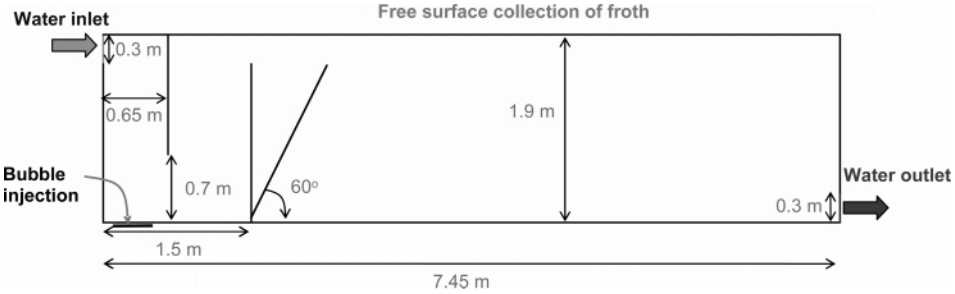

Figure 1. Flotation tank geometry.

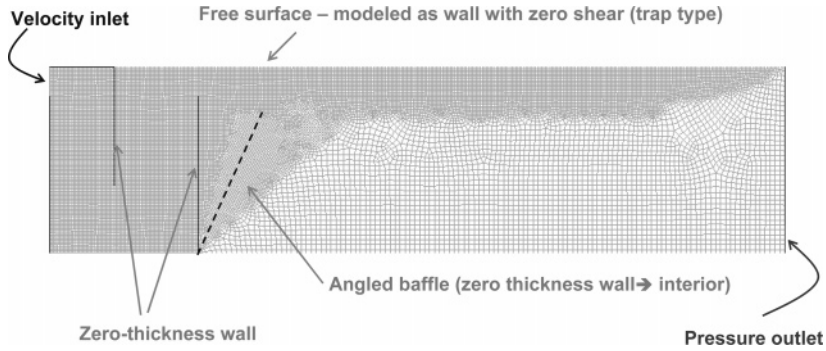

Figure 2. Grid of flotation tank.

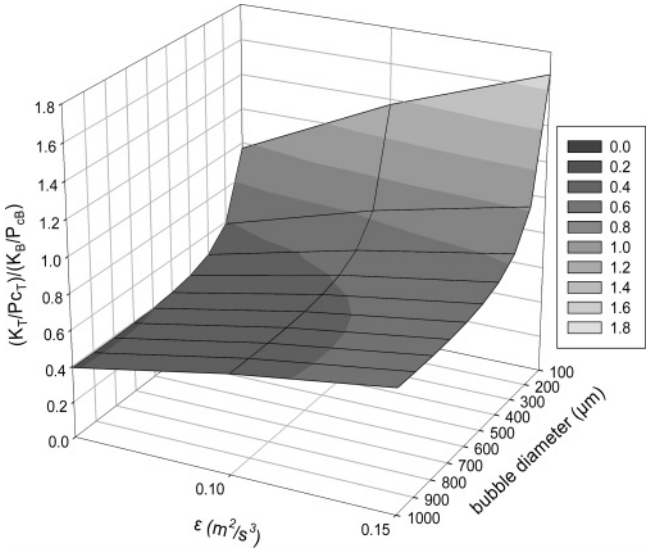

Figure 3. Ratio of turbulent-to-buoyant encounter frequency as a function of turbulent energy dissipation rate and bubble diameter. The particle size is 3 μm.

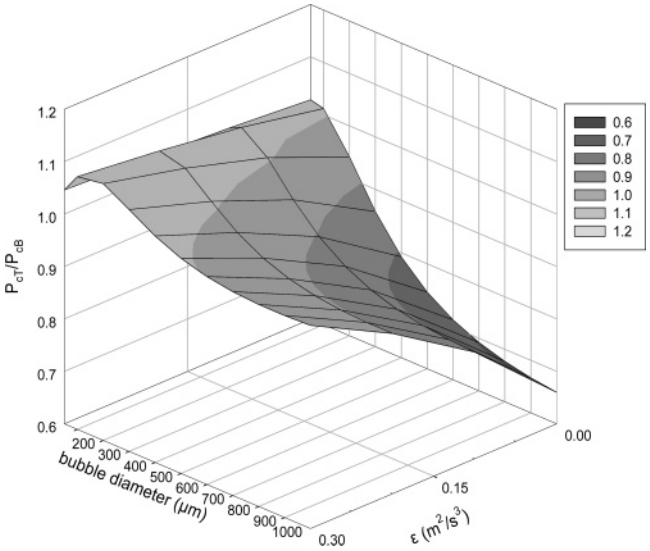

Figure 4. Ratio of turbulent-to-buoyant collision efficiency as a function of turbulent energy dissipation rate and bubble diameter. The particle size is 3 μm.

for uniform flow gives qualitatively similar results which are acceptable for the simple model developed here. So, the collision efficiency for the turbulent mechanism will be

$$P_{cT} = \left(\frac{3}{2} + \frac{4}{15}\left(\frac{2R_b W\rho}{\mu}\right)^{0.72} + 37.5\varphi\right)\left(\frac{R_p}{R_b}\right)^2 \qquad (9)$$

where the volume fraction dependent term has been also added.

The total collision frequency is computed by simply adding the collision frequencies for the three mechanisms i.e.:

$$K = K_B + K_G + K_T \qquad (10)$$

Apparently, the simple addition of terms is an approximation ignoring the interaction between the mechanisms. The two first mechanisms may be combined to a single one with a composite collision efficiency. This has been the usual approach in literature, but it can be proved that it is completely equivalent to the present treatment. The further incorporation of the third mechanism leads to questionable results with respect to the collision efficiencies[20] or to very complicated expressions.[10] For the purpose of the present work the simple linear addition appears to be a satisfactory choice. It is noted that the particle/bubble detachment process considered by many authors for cases of intense turbulent flotation can be ignored for the low turbulence levels met in DAF processes.

Fluid Dynamics. In the general case, flotation is a three phase problem and requires independent sets of momentum equations for the liquid, gas, and solid phases. However, for DAF applications in water and wastewater treatment the mass and volume fractions of particles are very small, and, in addition, their size is too small for considerable sedimentation so the solid phase can be treated as a passive scalar. So the problem is to solve the two phase problem for the gas and the liquid phase.

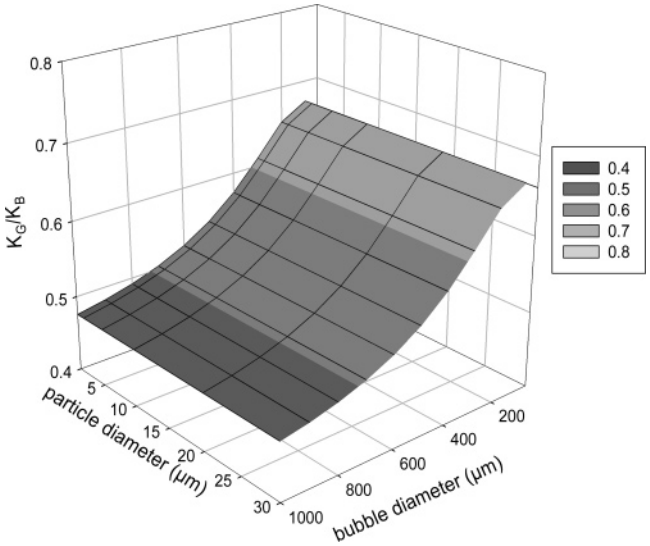

Figure 5. Ratio of gravitational-to-buoyant collision frequency as a function of particle and bubble diameters.

In most commercial CFD codes there are three different approaches to deal with the problem:[22] (i) The Lagrangian-Eulerian approach is of stochastic nature and consists of following the trajectories of bubbles one by one. This is the most accurate one and has a great success in simulating the real bubble column behavior,[23] but it is very time-consuming and at least the editions offered by the commercial CFD codes cannot be used for high gas volume fractions (>0.1) or when bubble trajectories are captured inside recirculation flow loops. (ii) The two-fluid Eulerian−Eulerian approach is a deterministic one and consists of considering the two phases as interpenetrating continua with their own set of momentum equations. Despite the effort that has been spent on the method there is not a generally accepted version ensuring realistic results. The method is still under development, and it is greatly based on empiricism.[24] (iii) The third approach is that of the mixture of phases which is also a deterministic one of Eulerian type. This method assumes that all phases behave as a mixture and solves only one set of momentum equations, that for the mixture velocity. All other variables are found from those of the mixture using standard algebraic relations. Evidently, this approach has all the disadvantages of the previous one, and, in addition, its accuracy to reconstruct complicated two phase flows is limited. On the other hand, it is by far less computationally demanding. Moreover, it has been shown (see the section of numerical model setup) that the mixture approach is quite suitable for the present application, so in the spirit of maximizing the simplicity and computational efficiency this approach is adopted here. Based on the fact that for the mixture approach the addition of a third phase does not increase the computational cost significantly, particles can be assumed as a separate third phase which offers some advantages in presenting and analyzing the simulation results.

Particle Conservation. In principle, the flotation problem should be formulated as a population balance for the distribution of the amount of particle mass attached on the bubbles. A simplified approach has been proposed[25] for batch flotation. According to these authors there is an upper limit on the mass of attached particles on a bubble. So, every moment there are "saturated" and "unsaturated" bubbles in the tank with only the "unsaturated" ones being able to further contribute to flotation. This approach has been used[9] in combination with CFD for a laboratory flotation cell. Whereas a model of this type is necessary to account for the reduction of available surface area for flotation in mineral applications where the particle mass loading is high, this is not the case for DAF where the particle mass loading is low so the "saturation" limit of the bubbles is never reached. In view of the fact that the amount of attached particles is not enough to change the bubble properties (e.g., effective density) one can avoid keeping track of the particles attached on the bubbles. This more simplified approach has been followed[8] for batch flotation. But for the case of continuous flotation considered here the situation is not so simple. There may be particles attached on bubbles leaving the system through the tank's main outlet (not from the froth) and which must be also taken into account for the computation of the particle removal efficiency. Of course, a well-designed flotation tank does not admit bubbles leaving the system through the main outlet. Here the assumption of a hydrodynamically well-designed cell is adopted implying a two-step design of the system: a purely hydrodynamic (bubble trajectories) and a hydrodynamic-physicochemical one (particle removal efficiency). So, according to the above the only modification to the CFD code is to add the loss term KN_pN_b (where N_p and N_b are the local particle and bubble concentrations, respectively) to the particle conservation equation. The removal efficiency is computed as the ratio of the difference between the incoming and outcoming particles over the incoming particles.

Another important question is how the flotation rate is computed in the CFD code. The relations for U_B and u_p given above are used only to show indicative results in stagnant liquid. In the code, the magnitudes of the difference between the bubble and the liquid velocity vectors and between the particle and the liquid velocity vectors are used instead of U_B and u_p, respectively. The second difference must be equivalent to the settling velocity, but the first one may include an additional relative motion of the bubble due to its inertia. The local gas hold up φ and turbulent energy dissipation rate needed for the computation of the local flotation frequency are computed by the CFD code.

Case Study

DAF Tank. The geometrical details of the DAF tank are shown in Figure 1. The main dimensions of the tank are 7.45 m long and 1.9 m high, the same as those used by Fawcett.[3] These dimensions are typical of industrial DAF tanks.[26] There are two vertical baffles near the water inlet of the tank to control the fluid flow. The one on the left is fixed vertically, whereas the one on the right can be set either vertical (90°) or inclined at certain angles. The baffle angles tested in this work are 90° and 60°. Due to the baffles' arrangement, the liquid which enters the tank is forced to travel first through a downflow section and then through an upflow section. These two sections constitute the reaction zone of the tank. Solid particles enter the tank as a homogeneous mixture with the incoming water.

To cope with a real application where heavy metals are initially absorbed on minute zeolite particles which are then removed by flotation,[27,28] the solids chosen for the present simulations are zeolite. Zeolite particles of 3 μm and 10 μm in diameter (D_p) and a density of 2000 kg/m^3 are employed. Their concentration is 1 kg solids per m^3 of incoming water which for the tested liquid flow rates yields volumetric fractions at the tank inlet below 10^{-3}.

The location for an efficient bubble injection in the tank is a serious matter of concern that has been dealt with in a previous study.[13] Among the several tested configurations the most efficient one is to introduce air through a series of nozzles at the left bottom corner of the tank, i.e., just below the liquid

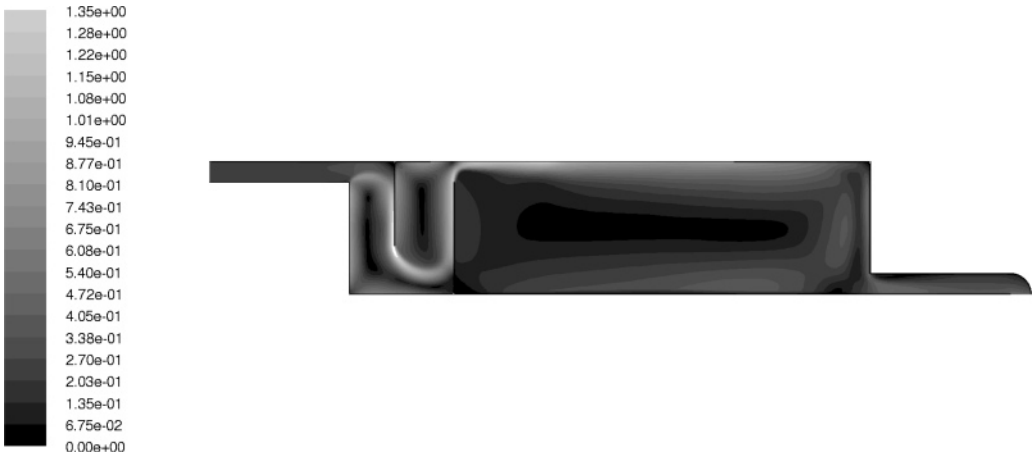

Figure 6. Typical fluid velocity contour plots for the case $D_b = 100$ μm, $D_p = 3$ μm, $G = 0.2$ kg/(m^{3}s), $U_L = 0.26$ m/s.

entry region (Figure 1). This configuration is used here. Air is introduced as individual bubbles of 100, 200, and 500 μm in diameter (D_b) (one size at a time). Gas flow rate (G) is set at 0.1 and 0.2 kg/m^{3}s (4.1×10^{-3} and 8.2×10^{-3} m^3/s, respectively), values warranting that the local air volume fraction is always below ~10% inside the tank.

Given the relatively strong tendency of large bubbles to float, the liquid flow rate should be selected high enough so as to provide sufficient downflow above the gas injection location to slow down the ascending bubbles and thus increase their residence time in the tank. Moreover, high liquid flow rates yield increased turbulence levels that promote bubble/particle collisions. On the other hand, the liquid flow rate must not be too high to avoid breakup of bubble/particles aggregates and also avoid carryover of aggregates to the tank outlet. After extensive trials it is decided that most of the present runs to be performed with an inlet liquid velocity (U_L) of 0.26 m/s (0.09 kg/s). This corresponds to a hydraulic load of approximately 45 m/h which is a value above the normal conditions for DAF operation but which has been successfully employed in the past for this particular tank design.[3] To appraise the effect of liquid flow rate, runs with 0.13 and 0.52 m/s inlet liquid velocity are also conducted for a particular set of conditions.

Numerical Model Setup. To model the flow in the present flotation tank, the code FLUENT 6.2.16 is used. The modeling procedure involves two steps. The first step involves building the grid using GAMBIT preprocessor and imposing the boundary conditions on the model. All the model and solution parameters are fixed to obtain a solution using FLUENT solver in the second step. A total number of 29 071 cells are used to discretize the computational domain being denser in regions of more intense activity, Figure 2.

As explained above, the so-called *Mixture model*[22] is employed to solve the flow field. The suitability of this model was initially endorsed by the fulfillment of certain criteria proposed by FLUENT regarding particle loading and particle Stokes number.[29] Furthermore, it was shown[12,14] that the *Mixture model* produced similar results with the two-fluids Eulerian−Eulerian model, indicating that the two models perform comparably for our application. With both of these models it is imperative to have the inlet and outlet of the flow not directly imposed to the tank but instead use a phantom entrance and exit pipeline (diameter 0.3 m, length 1.7 m) to overcome the abrupt disturbance of the velocity profile at these points.

The boundary condition for the tank inlet is the prescribed inlet water velocity with 10% turbulence intensity. The boundary condition for the outlet is the pressure at the exit of the tank with 10% backflow turbulence intensity and reference pressure the hydrostatic value. The free surface of the tank is modeled as a wall with zero shear that acts as a sink for the gas phase. The remaining walls are modeled as fixed walls with a zero near surface velocity. The *standard k-ω* turbulence model is used to describe the turbulence inside the tank. The selection of the boundary condition for the free surface of the tank and the turbulence model is based on the success of earlier tests among several reasonable options.[12,14] Drag coefficients are estimated by the model of Schiller and Naumann (1935) proposed as default by FLUENT[22] for general use for any fluid−fluid pairs of phases.

The implicit segregated model is employed to solve the governing equations, whereas the pressure-velocity coupling is discretized by the SIMPLE algorithm. Convergence is assumed accomplished if continuity varies by less than 10^{-6} in the iterations. Since there is no net flow across the tank and in order to reduce the computational effort, a 2D frame of reference is employed.

Results and Discussion

Before the presentation and discussion of the simulation results it is important to get an idea of the relative contribution of the individual mechanisms to the total flotation rate under the conditions of the simulations. From the CFD calculations it is found that the turbulent energy dissipation rate is of the order of 0.1 m^2/s^3 in the reaction zone of the tank so values of ϵ of this order are used for the comparison of the flotation mechanisms. The ratio between the turbulence and buoyancy induced encounter frequencies is shown in Figure 3for a range of ϵ and bubble diameters typical for the foregoing simulation. Results are for 3 μm particles. As it is expected this ratio increases as ϵ increases and bubble size decreases. Looking at the figure, one is further tempted to argue that for bubbles larger than ~200 μm buoyant encounters prevail for the entire range of the examined turbulent energy dissipation rates. However, due to the fair accuracy of simple flotation models in describing complex flotation processes, it is more prudent to claim that this ratio is of the order of unity which means that the two encounter frequencies have comparable magnitudes.

To get the whole picture, the corresponding collision efficiencies must be also considered. The ratio of the two collision efficiencies is displayed in Figure 4. Evidently, the ratio of the efficiencies is also of the order of unity which means that the turbulent and buoyant collision rates are comparable, and none of them can be ignored for the simulation of the flotation

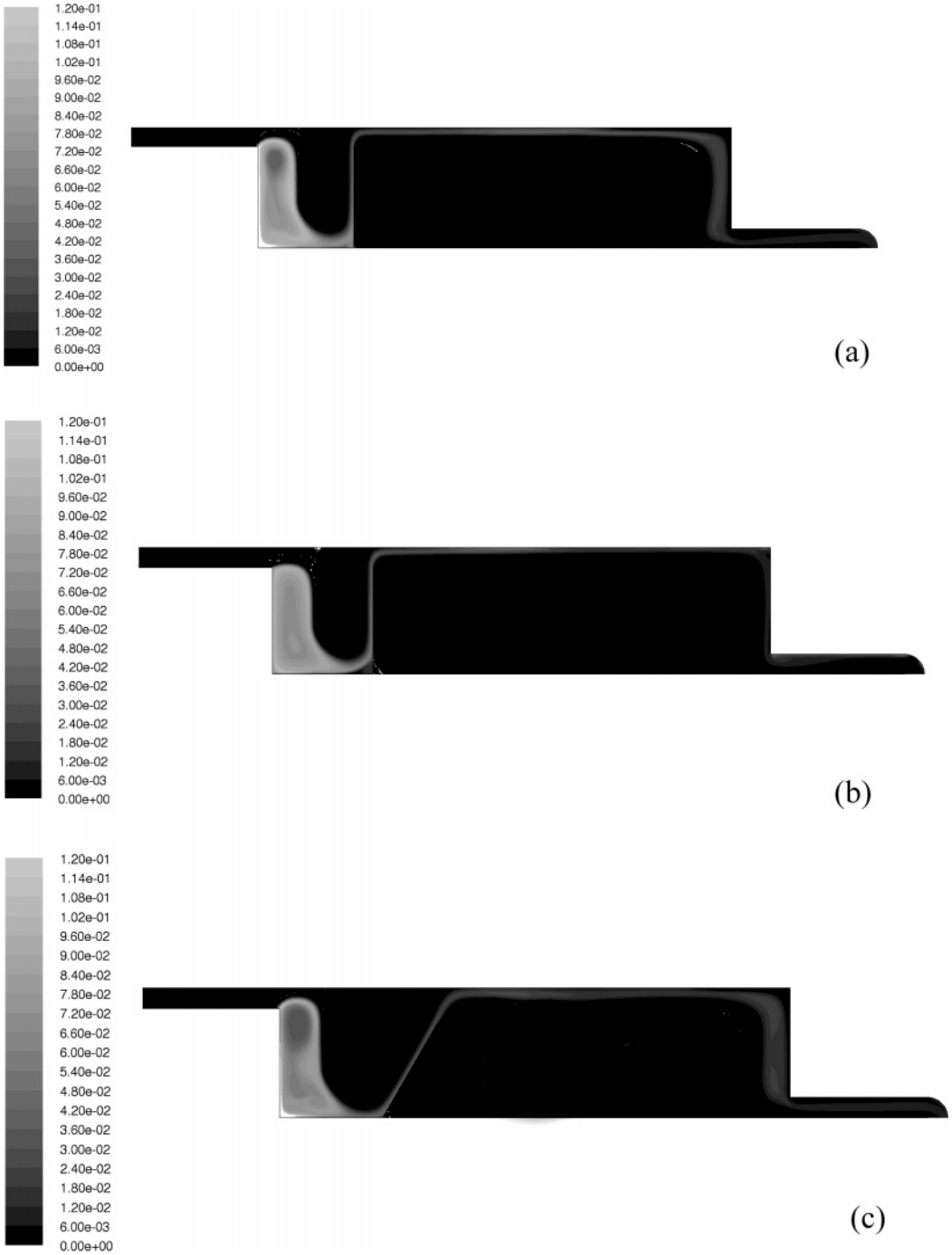

Figure 7. Gas volume fraction (φ) contour plots for U_L: 0.26 m/s $D_p = 3$ μm and (a) $D_b = 100$ μm, $G = 0.1$ kg/(m^{3}s); (b) $D_b = 200$ μm, $G = 0.1$ kg/(m^{3}s); and (c) $D_b = 100$ μm, $G = 0.1$ kg/(m^{3}s). The baffle is vertical for cases (a) and (b) and inclined for case (c).

process. This is especially true for the smaller bubbles typical for DAF applications.

Next, the contribution of the gravitational motion of the particles is examined. At first glance one may think this is insignificant compared to the buoyant term since the ratio of the bubble-to-particle velocity is of the order two with respect to the ratio of the bubble-to-particle size. But the ratio of the collision efficiencies exhibits the inverse order with respect to the size ratio. The outcome is that the ratio of the collision frequencies corresponding to the two mechanisms is pretty constant. The ratio of the gravitational to buoyant collision frequencies is shown as a function of bubble size (100−1000 μm) and particle size (1−30 μm) in Figure 5. It is evident that the ratio does not depend on particle size and exhibits only a small sensitivity to bubble size ($K_G/K_B \approx 0.55 \pm 0.1$). Conclusively, the gravitational collision mechanism is comparable to the buoyant one for the entire range of the examined parameters so it must be also taken into account in the simulation.

Before looking into the results of the particle removal efficiencies under different operating conditions it is useful to see some typical fields of the main variables. This will help appreciate the significance of the hydrodynamics in the tank for the determination of the particle removal efficiency. Figure 6 presents a typical liquid velocity flow field in the tank. The general pattern is the same for all the examined cases. There are three large recirculation zones in the tank: a first between the entrance and the first baffle, a second between the two baffles, and a third (larger) between the second baffle and the outlet of the tank. The major fluid transfer from the inlet to outlet of the tank occurs through a narrow stream exhibiting

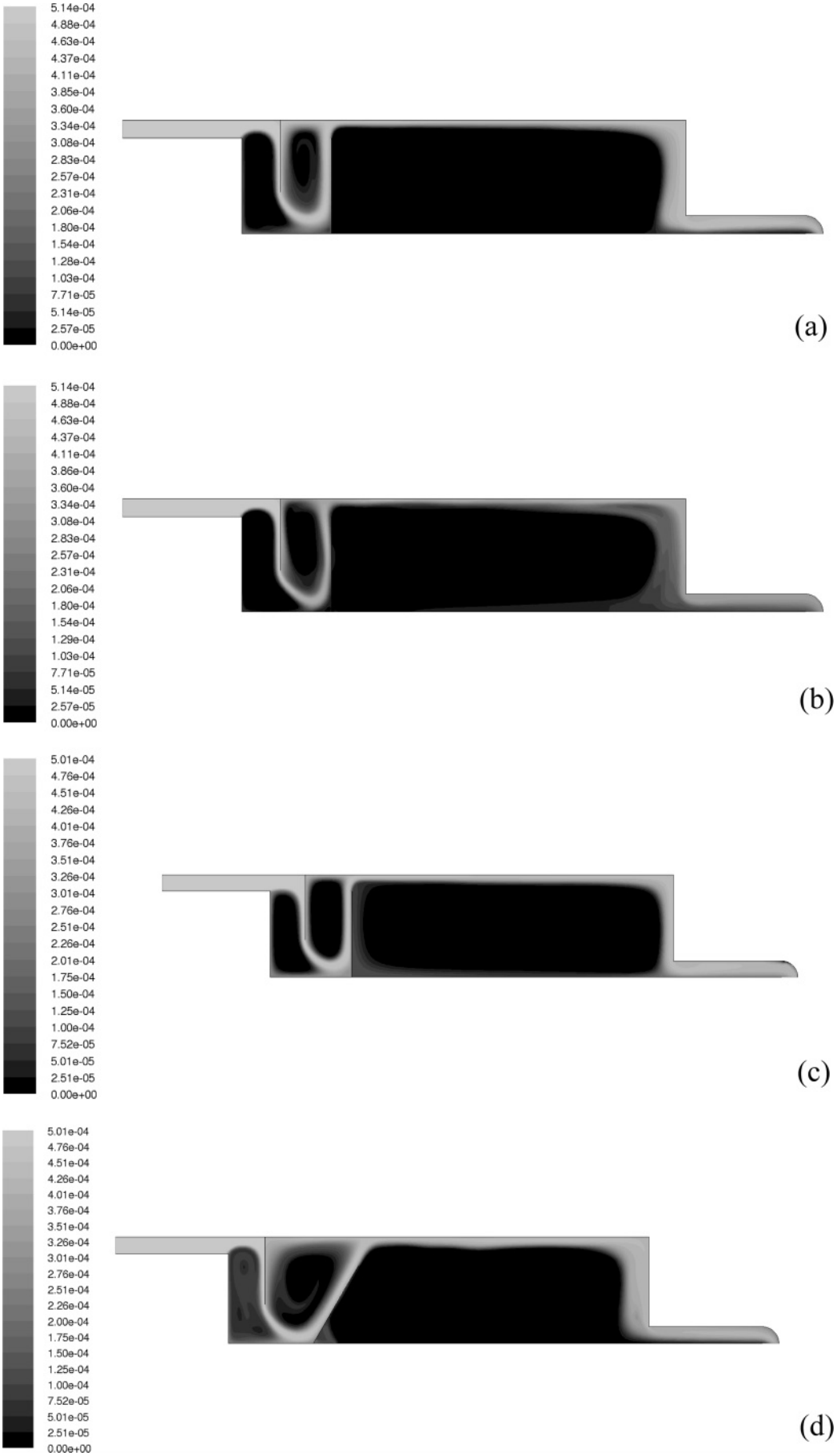

Figure 8. Particle volume fraction contour plots for U_L: 0.26 m/s and (a) $D_b = 100\ \mu$m, $D_p = 3\ \mu$m, $G = 0.1$ kg/(m^{3}s); (b) $D_b = 100\ \mu$m, $D_p = 10\ \mu$m, $G = 0.1$ kg/(m^{3}s); (c) $D_b = 200\ \mu$m, $D_p = 3\ \mu$m, $G = 0.1$ kg/(m^{3}s); and (d) $D_b = 100\ \mu$m, $D_p = 3\ \mu$m, $G = 0.1$ kg/(m^{3}s). The baffle is vertical for cases (a)−(c) and inclined for case (d).

very high velocities (to fulfill the continuity equation). This narrow stream consists of boundary layers (nearby the two baffles), stagnation points (attachment onto the baffles), and free jet flow regions (between the baffles).

The gas volume fraction (hold up) contours in the tank are shown in Figure 7 for three indicative cases. There is a high hold up region in the first recirculation zone. This is the region where the bubbles are injected from the bottom of the tank. After leaving this region the bubbles follow the main fluid stream until they reach the free surface. For the smaller bubbles (100 μm, Figure 7a,c) which follow more persistently the fluid streamlines there is a low hold-up region in the center of the first recirculation zone and also some bubbles are dragged by the liquid flow to the tank outlet. As it is expected the stronger buoyancy of the larger bubbles (200 μm, Figure 7b) tends to alleviate both problems. In an earlier study,[11] bubbles larger than 500 μm were found to deviate appreciably from the narrow main fluid stream leading to a broader reaction zone but at the cost of a less uniform gas hold up in the first recirculation zone. Furthermore, when three sizes of simultaneously fed bubbles (200, 500, and 1000 μm) were examined using a Langragian-Eulerian model, bubbles appeared to spread even better and occupy more space in the two first recirculation zones of the tank, while all sizes deviated significantly from the main flow stream yielding a much broader reaction zone.[13] In real applications the coexistence of different sizes of bubbles in the tank is the rule so such improved performance is expected. Nevertheless, since the scope of this work is to demonstrate the merits of the proposed CFD model in cases where several flotation mechanisms contribute to the particles removal, simulations are restricted herein to a single bubble size every time.

The estimated solid volume fraction in the tank for several indicative cases is shown in Figure 8. Inspection of the spatial profiles of the variables computed from the CFD code in Figures 6−8 lead to the following general picture for the fate of the particles entering the flotation tank. At first, some particle-bubble attachment occurs at the boundary between the narrow main fluid stream and the gas in the first recirculation zone. However, the most effective mixing of bubbles with particles occurs in the free jet of the fluid as it leaves the first baffle so this is actually the main "reaction zone". The attachment continues but at lower rates in the main liquid stream carrying bubbles and particles over the second baffle, until eventually the bubbles reach the free surface. The particles that remained unattached follow the fluid flow toward the tank outlet. The above discussion reveals the domination of the hydrodynamics on the flotation process.

Table 1 presents collectively all the conditions for which simulations are performed along with the computed particle removal efficiencies. It is evident that the removal efficiency increases as the bubble size decreases for a given gas flux entering the tank. This is in accordance with the traditional theories for the local flotation rate. The situation appears more complex when increasing the gas flux while keeping constant the bubble size. The removal efficiency always increases with the gas flux but for the case of the larger (500 μm) bubbles this increase is quite insignificant. This is the first evidence that the combination of large scale hydrodynamics with local flotation rates can lead to results very different than that of the traditional flotation theory. The increase in the local flotation rate with the gas flux is due to the increase of bubbles population and also to the term in the collision efficiencies depending on the gas volume fraction. But this increase of the local rate is not sufficient to raise the total efficiency for the larger (500 μm) bubbles which have limited residence time in the tank.

Table 1. Total Particle Removal Efficiencies for All the Conditions Examined in the Present Simulations

bubble diameter D_b, μm	particle diameter D_p, μm	baffle position	gas mass flow rate G, kg/(m^{3}s)	liquid inlet velocity U_L, m/s	removal efficiency, %
100	3	vertical	0.1	0.26	67.15
			0.2		87.56
		angled	0.1		58.76
			0.2		83.44
	10	vertical	0.1		69.13
			0.2		87.50
		angled	0.1		60.99
			0.2		83.73
200	3	vertical	0.1	0.26	9.97
				0.13	16.93
				0.52	9.08
			0.2	0.26	16.83
		angled	0.1		11.36
			0.2		20.44
	10	vertical	0.1		29.46
			0.2		51.27
		angled	0.1		38.17
			0.2		55.18
500	3	vertical	0.1	0.26	6.30
			0.2		6.84
		angled	0.1		7.67
			0.2		8.28
	10	vertical	0.1		21.36
			0.2		21.64
		angled	0.1		8.10
			0.2		11.81

The effect of the liquid inlet velocity is rather clear. Increasing the fluid velocity increases the turbulence levels promoting the turbulent mechanism of flotation but most importantly leads to reduction of the residence time in the tank and, thus, to reduced removal efficiencies. This behavior is clearly depicted in Table 1 where the removal efficiency decreases as the liquid inlet velocity increases for the case of 200 μm bubbles. However, the suppression of the particle removal efficiency is not linear with the increase of the liquid velocity. It seems that at lower liquid velocities (higher removal efficiencies) the effect is more pronounced. On the contrary, the effect of the baffle inclination is very complex and depends on the particular conditions of the simulation; it can either increase or decrease the total removal efficiency.

According to local flotation rate theories, flotation rate should increase with particle size since the latter appears in the numerator of the collision efficiency relation for the turbulent and buoyant mechanisms as well as in the settling velocity term for the gravitational mechanism. The increase of the removal efficiency with particle size is evident in Table 1 but only in cases where the removal efficiency is small. In such cases, improving the local flotation rate enhances the total particle removal. On the contrary, in cases where the removal efficiency is already high enough, the controlling step for its determination is not the local flotation rate but the local hydrodynamics of the tank. Thus, for the 100 μm bubbles case (see Table 1 and Figure 8a,b) where the removal efficiency is above ~67% already with the 3 μm particles, using larger particles does not virtually affect the total removal efficiency although the local flotation rate is undoubtedly increased. This is because the removal efficiency in this case is dictated mainly by the hydrodynamic details of the narrow main liquid stream traveling adjacent and in between the two baffles. Apparently, DAF tanks constitute an interesting application where the absence of external mixing requires careful

manipulation of other operational or/and geometrical parameters in order to achieve adequate interaction of the incoming fluid (carrying the particles) with the injected bubbles.

Conclusions

Under conditions encountered in large scale flotation tanks with no means of external agitation of the fluid suspension (low turbulent energy dissipation rates), the buoyant motion (rising) of the bubbles, the gravitational motion (settling) of the particles, and turbulence appear to have comparable contribution in determining the local flotation rates. This is particularly true for bubbles smaller than 200 μm and for particle sizes less than 30 μm, conditions common in water and wastewater DAF applications. The performed CFD simulations reveal certain key characteristics of the hydrodynamics in the present DAF tank that play a role in determining the local flotation rates. The most prominent characteristics are as follows: (a) the existence of three recirculation loops, one between the left side wall and the first baffle, a second in between the two baffles, and a third (and larger one) between the second baffle and the right side wall, (b) a narrow fast liquid stream carrying most of the liquid and particles in the reaction zone which is either sliding along the baffles or flowing as a free jet between the baffles, and (c) regions of high gas hold-up (first recirculation loop) and low gas hold-up (second and third recirculation loops). The suggestion based on the simulation results is that small bubbles at a high gas flux and a vertical baffle must be used for higher removal efficiency in the present DAF tank. But the most important observation is that the interaction between the tank hydrodynamics and the local flotation kinetics is very complicated, and it can lead to results for the total removal efficiency which could never be inferred simply from flotation theories. Thus, the combination of flotation theories for the local flotation rates with CFD models seems an appropriate tool for the design of large scale DAF equipment.

Literature Cited

(1) King, R. P. *Modeling and simulation of mineral processing systems*; Butterworth-Heinemann: London, 2001.

(2) Nguyen, A. V.; Schulze, H. J. *Colloidal Science of Flotation*; Marcel Dekker: New York, 2004.

(3) Fawcett, N. S. J. The hydraulics of flotation tanks: computational modelling. In *Dissolved Air Flotation*, Proceedings of the International Conference Chartered Institute of Water and Environmental Management, London, 1997; pp 51−71.

(4) Hague, J.; Ta, C. T.; Biggs, M. J.; Sattary, J. A. *Small scale model for CFD validation in DAF application*. In The 4th International Conference Flotation in Water and Waste Water Treatment; Helsinki, September 11−14, 2000, Session 6.

(5) Ta, C. T.; Beckley, J.; Eades, A. *A multiphase CFD model of DAF process*. In The 4th International Conference Flotation in Water and Waste Water Treatment; Helsinki, September 11−14, 2000, Session 6.

(6) Desam P. R.; Datta A.; Moerse W.; Miller J. D. A *Computational Fluid Dynamics (CFD) Model for a bubble separation tank used in wastewater treatment*. In Proceedings of XXI International Mineral Processing Congress; Rome, Italy, June 23−28, 2000.

(7) Koh, P. T. L.; Manickam, M.; Schwarz, M. P. CFD simulation of bubble-particle collisions in mineral flotation cells. *Miner. Eng.* **2000**, *13*, 1455.

(8) Koh, P. T. L.; Schwarz, M. P. CFD modeling of bubble-particle collision rates and efficiencies in a flotation cell. *Miner. Eng.* **2003**, *16*, 1055.

(9) Koh, P. T. L.; Schwarz, M. P. *CFD modeling of bubble-particle attachments in a flotation cell*. In Proceedings of Centenary of Flotation Symposium; Brisbane, Australia, June 2005, pp 201−207.

(10) Kostoglou, M.; Karapantsios, T. D.; Matis, K. A. Modeling local flotation frequency in a turbulent flow field. *Adv. Colloid Interface Sci.* **2006**, *122*, 79.

(11) Emmanouil, V.; Skaperdas, E.; Karapantsios, T. D.; Matis, K. A. *Comparison of multiphase and turbulence models in simulating the performance of a dissolved air flotation*. In Proceedings of the Southeastern Europe Fluent Event 2005; Halkidiki, Greece, May 11−13, 2005.

(12) Emmanouil, V.; Skaperdas, E; Karapantsios, T. D.; Matis, K. A. *Towards three-phase modeling of a dissolved air flotation tank*, XXIII International Mineral Processing Congress; Istanbul, Turkey, September 3−8, 2006.

(13) Emmanouil, V.; Skaperdas, E.; Karapantsios, T. D.; Matis, K. A. Two-phase simulations of an off-nominally operating dissolved air flotation tank. *Int. J. Environ. Pollut.* **2007**, *30* (2), 213.

(14) Emmanouil, V.; Karapantsios, T. D; Matis K. A. Two and three-Phase Simulations of an ill-functioning dissolved air flotation tank. *Int. J. Environ. Waste Manage*. In press.

(15) Yoon, R. H.; Luttrell, G. H. The effect of bubble size on fine particle flotation. *Miner. Process. Extr. Metall. Rev.* **1989**, *5*, 101.

(16) Nguyen, A. V. Hydrodynamics of liquid flows around air bubbles in flotation: a review. *Int. J. Miner. Process.* **1999**, *56*, 165.

(17) Bathelor, G. K. *The theory of homogeneous turbulence*; Cambridge University Press: New York, 1953.

(18) Saffman, P. G.; Turner, J. S. On the collision of drops in turbulent clouds. *J. Fluid Mech.* **1956**, *1*, 16.

(19) Pyke, B.; Fornasiero, D.; Ralston, J. Bubble particle heterocoagulation under turbulent conditions. *J. Colloid Interface Sci.* **2003**, *265*, 141.

(20) Bloom, F.; Heindel, T. J. On the structure of collision and detachment frequencies in flotation models. *Chem. Eng. Sci.* **2002**, *57*, 2467.

(21) Pnueli, D.; Gutfinger, C.; Fichman, M. A turbulent-Brownian model for aerosol coagulation. *Aerosol Sci. Technol.* **1991**, *14*, 201.

(22) *FLUENT 6.1 User's Guide*; Fluent Inc.: 2003.

(23) Van den Hengel, E. I. V.; Deen, N. G.; Kuipers, J. A. M. Application of coalescence and breakup models in a discrete bubble model for bubble columns. *Ind. Eng. Chem. Res.* **2005**, *44*, 5233.

(24) Jakobsen, H. A.; Lindborg, H.; Dorao, C. A. Modeling of bubble column reactors: progress and limitations. *Ind. Eng. Chem. Res.* **2005**, *44*, 5107.

(25) Bloom, F.; Heindel, T. J. Modeling flotation separation in a semi-batch process. *Chem. Eng. Sci.* **2003**, *58*, 353.

(26) O'Neill, S.; Yeung, H.; Oddie, G. Physical modelling study of the dissolved air flotation process. In *Dissolved Air Flotation*, Proceedings of the International Conference Chartered Institute of Water and Environmental Management, London, 1997; pp 75−81.

(27) Matis, K. A.; Zouboulis, A. I.; Gallios, G. P.; Erwe, T.; Blocher, C. Application of flotation for the separation of metal-loaded zeolites. *Chemosphere* **2004**, *55*, 65.

(28) Zamboulis, D.; Pataroudi, S. I.; Zouboulis, A. I.; Matis, K. A. The application of sorptive flotation for the removal of metal ions. *Desalination* **2004**, *162*, 159.

(29) Emmanouil, V. CFD simulation of the flotation process. M.S. Thesis, Aristotle University of Thessaloniki, Greece, 2004 (in Greek).

Received for review March 16, 2007
Revised manuscript received June 5, 2007
Accepted July 20, 2007

IE0703989